Simplified Over-the-Air Noise Figure Measurement Method for Reduced Uncertainty

Anouk Hubrechsen[1,2*], Tim Stek[1,2*], A. Bart Smolders[1,2]
[1]Department of Electrical Engineering, Eindhoven University of Technology, The Netherlands
[2]Antennex B.V., The Netherlands
a.hubrechsen@tue.nl

***Abstract*— Receiving systems for mm-wave applications are increasing in complexity and level of integration. Therefore, crucial metrics such as noise figure have to be characterized using an over-the-air approach. We introduce a simplified version of the reverberation-chamber noise-figure (RCN) method, such that two instead of three calibration steps are necessary for the measurement of noise figure and gain. This reduces measurement uncertainty and removes the need to use a vector network analyzer, so all measurements can be performed with a spectrum analyzer. We show that the measured noise figure results and reference value are within each others uncertainty bounds within the 24-28.5 GHz frequency range, validating the use of this method. By using the simplified RCN, the expanded uncertainty reduced from 0.67 dB to 0.37 dB for the noise figure measurement, and from 1.00 dB to 0.75 dB for the gain measurement.**

***Keywords*— mm-wave, noise figure (NF), over-the-air (OTA) measurements, reverberation chambers (RC), RCN, wireless system.**

I. Introduction

Noise figure (NF) is a crucial metric in various receiving systems, such as those used in radio astronomy and telecommunications, among numerous other wireless applications [1], [2]. In many of these applications, the device has a high level of integration, where the LNA and antenna cannot be taken apart. This has the benefit that the system architecture can be optimized using noise matching, but it has a drawback of only being able to characterize the system NF with over-the-air (OTA) methods. Especially in the millimeter (mm)-wave domain, this raises the measurement complexity significantly.

There are existing methods for OTA measurements of NF. The most notable being the radiometric method [3], [4], which is based on a Y-factor method, and the gain-to-noise-temperature (G/T) method [5], [6]. The sensitivity to errors of both of these methods increases significantly at mm-wave, due to their dependency on device positioning, radiation pattern, and form factor [7]. Additionally, the radiometric method depends on a detailed sky noise model that becomes significantly less accurate above 10 GHz [8]. Recently, the reverberation-chamber noise-figure (RCN) method was introduced to overcome these drawbacks [9]. This method combined the radiometric method with a reverberation chamber (RC), to create a hot and cold noise environment in a repeatable manner. Due to the inherent properties of the RC, a wireless device can be placed almost anywhere in the chamber, regardless of form factor and orientation [10].

In this paper, we introduce a simplified version of the RCN which requires two calibration steps instead of three. This is accomplished by placing both the Device Under Test (DUT) and a calibration antenna with a known efficiency in the chamber at the same time. This removes the need to perform a pre-characterization of the transfer function and noise figure of the RC with a vector network analyzer. In the simplified RCN, all measurements can be performed with a spectrum analyzer, making it more user-friendly. The simplification also reduces the overall measurement uncertainty due to the need for one less calibration measurement. We compare the result with a reference measurement, and with the original RCN, both obtained from [9]. The simplified RCN is described in Section II. Section III focuses on the measurement setup and uncertainty, including measurement results. The work is concluded in Section IV.

II. Simplified RCN: Theory

The simplified RCN does not require chamber pre-characterization, in which the transfer function, G_{ref}, and the NF of the chamber are determined with a vector network analyzer. Instead, we use a calibration antenna with a known efficiency to estimate the noise-power level inside the chamber. Since the power transfer through an RC is constant when averaged over enough mode-stirring samples (with some uncertainty due to a lack of spatial uniformity, which is taken into account in the uncertainty analysis), this can be used to extract the DUTs NF and gain, similar to [9]. The procedure is illustrated in Figs. 1 and 2.

The first measurement is a calibration measurement to determine the hot and cold noise-power levels in the chamber, P_{hot} and P_{cold}, respectively. This is needed for the noise-temperature measurement in the RC. We use an electronic noise source, which is a reversely biased diode and can be turned on and off to create two noise power levels. The noise source is connected to an amplifier and an antenna, Antenna 1, as shown in Fig. 1. The noise from the noise source is amplified to overcome the losses in the RC, and Antenna 1 is used to transmit the noise power into the RC. In the first calibration measurement, the DUT is placed inside the RC, which is terminated with a 50Ω load. Additionally, a calibration antenna, Antenna 2, with a known efficiency, $\eta_{\text{ant,2}}$, is placed in the chamber. The received power, P_{m}, is measured using a spectrum analyzer, and averaged over N mode-stirring samples, obtained by changing the position

[*] equal contribution

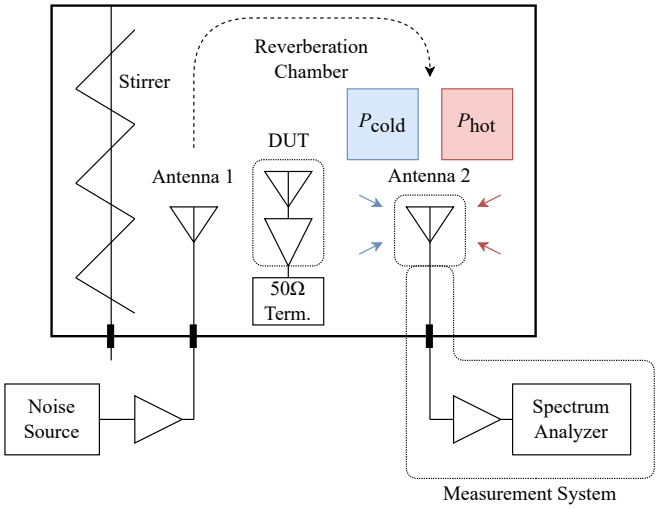

Fig. 1. Schematic overview of the first calibration Measurement.

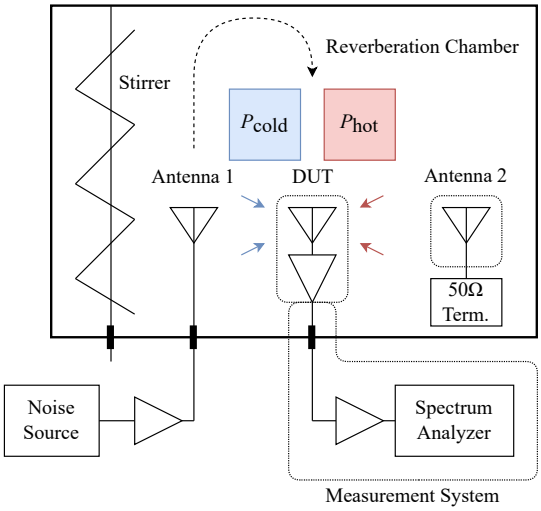

Fig. 2. Schematic overview of the DUT Measurement.

of the mode-stirring mechanisms. This is repeated for both noise-power levels according to [11].

The noise temperature, T_{meas}, and gain, G_{meas}, of the measurement system (the measurement system is illustrated in Fig. 1), and the total efficiency of Antenna 2, $\eta_{\text{ant,2}}$, should be subtracted from the measured power, to obtain the noise-power level at the aperture of Antenna 2, inside the chamber. The total efficiency can be obtained in a separate measurement campaign or by using a datasheet value, and T_{meas} and G_{meas} are estimated using a second calibration measurement. In that measurement, the noise source is connected to the measurement system and a Y-factor measurement is performed [9]. The hot and cold noise-power levels inside the chamber can now be calculated using

$$P_{\text{hot/cold}} = \frac{\langle P_{\text{m,hot/cold}} \rangle_N}{G_{\text{meas}} \eta_{\text{ant,2}}} - \text{k}_\text{B} \left(\frac{T_{\text{meas}}}{\eta_{\text{ant,2}}} + T_{\text{ant,2}} \right), \quad (1)$$

where k_B is Boltzmann constant, $\langle P_{\text{m,hot/cold}} \rangle_N$ is the measured output power, averaged over N mode-stirring samples, when the noise source is turned on and off, respectively, and $T_{\text{ant,2}}$ is the noise temperature of the calibration antenna, and is estimated using

$$T_{\text{ant,2}} = \frac{1 - \eta_{\text{ant,2}}}{\eta_{\text{ant,2}}} T_{\text{ph}}, \quad (2)$$

where T_{ph} is the physical temperature of the antenna.

After the two calibration steps, the DUT measurement can be performed. The DUT is connected to the measurement system and the calibration antenna is terminated with a 50Ω load. The DUT and antennas remain in the chamber for all measurements to keep a constant chamber transfer function. Therefore, the noise power levels P_{hot} and P_{cold}, at the input of Antenna 2 will be the same as the noise power levels at the input of the DUT. Next, the noise temperature, T_{DUT}, and gain, G_{DUT}, of the DUT can be estimated using the same approach as in [9]. The ratio $Y = \langle P_{\text{m,hot}} \rangle_N / \langle P_{\text{m,cold}} \rangle_N$ is used, where $P_{\text{m,hot}}$ and $P_{\text{m,cold}}$ are the measured power levels during the DUT measurement, when the noise source is turned on and off, respectively. With this power ratio, Y, the noise temperature of the DUT can be estimated using

$$T_{\text{DUT}} = \frac{P_{\text{hot}} - Y P_{\text{cold}}}{\text{k}_\text{B}(Y - 1)} - \frac{T_{\text{meas}}}{G_{\text{DUT}}}. \quad (3)$$

The gain of the DUT is calculated using

$$G_{\text{DUT}} = \frac{\langle P_{\text{m,hot}} \rangle_N - \langle P_{\text{m,cold}} \rangle_N}{P_{\text{hot}} - P_{\text{cold}}} \frac{1}{G_{\text{meas}}}. \quad (4)$$

Note that this method is independent of the chamber gain and noise figure, and of the efficiency Antenna 1. Next, we validate the simplified RCN method with measurements including uncertainty.

III. Measurement Setup, Results, and Uncertainty

As an active DUT we used a standard-gain horn antenna, connected to a 6 dB attenuator and an amplifier, as shown in Fig. 3, similar to [9]. We used this device as a DUT, such that we could use a reference measurement to compare the results with, which was the same approach as the one presented in [9]. We compare the results of this new simplified method to the results presented in [9] of the original RC noise figure (RCN) method, and to a reference measurement. In that work, the reference measurement for NF was obtained with a conducted Y-Factor measurement of the LNA, where the NF of the antenna was added using (2). The gain reference was obtained with a three-antenna efficiency method [12]. It should be noted that the DUT in this work used a waveguide-to-coaxial adapter with horn antenna of the same type, but not the exact same antenna-adapter combination as in [9]. The LNA used was the same.

The measurement is performed in the frequency band from 24 to 28.5 GHz. We used a resolution bandwidth of 1 MHz and a video bandwidth of 5 MHz. The dedicated mm-wave RC has a size of approximately 0.5 x 0.6 x 0.8 m^3, and the number of mode-stirring samples, N, was 100, which is sufficient for this

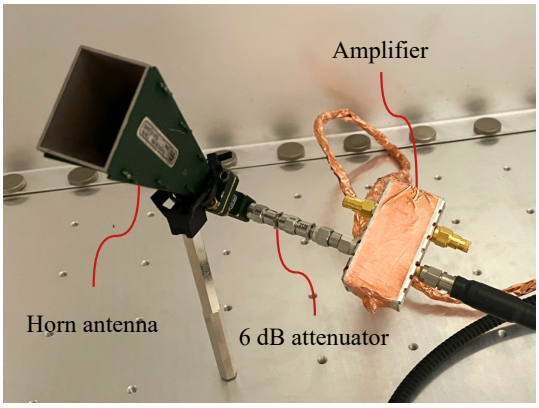

Fig. 3. Photograph of the DUT.

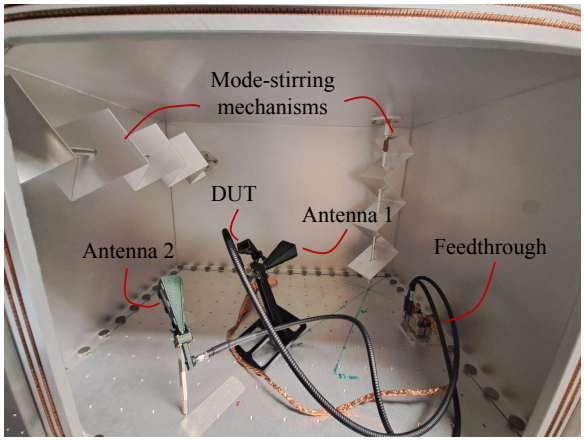

Fig. 4. Setup inside the RC.

application [9], [13]. The noise source we used had an excess noise ratio of 12 dB, the amplifier at the transmitting side had a gain of 40 dB, and the pre-amplifiers for the spectrum analyzer also had a total gain of approximately 40 dB. The noise source, amplifiers, power supplies, and spectrum analyzer are placed outside of the chamber, and connected to the antennas and DUT through a feedthrough panel. The complete setup is shown in Fig. 4.

The setup used was similar to the one used to validate the RCN presented in [9]. Therefore, many uncertainty contributions stayed the same. The uncertainties of each measurement are shown in Table 1. The uncertainty in the Y-factor measurement of the measurement system was the same as in [9]. Uncertainty contributions from the amplifiers, cables, noise source, and spectrum analyzer are taken into account here (2nd calibration measurement). Those same uncertainties are also taken into account in the first calibration measurement and the DUT measurement, with the addition of the chamber lack of spatial uniformity. The simplified RCN has no increased uncertainty due to the additional assumption on having a calibration antenna with a known efficiency, as the original RCN needed such an antenna as well. Therefore, they both have the same uncertainty contribution related to radiation efficiency. The simplified RCN does not

Table 1. Uncertainty of each measurement

Measurement	Uncertainty
1st Calibration Meas: $P_{\text{hot/cold}}$	0.13 dB
2nd Calibration Meas: NF	0.02 dB
2nd Calibration Meas: Gain	0.23 dB
Radiation Efficiency Calibration Antenna	1.39 %
DUT Measurement: NF	0.16 dB
DUT Measurement: Gain	0.20 dB

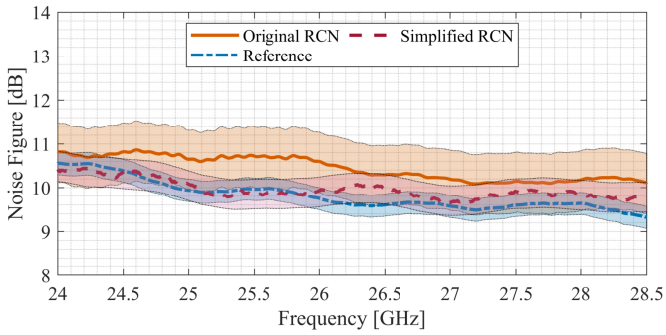

Fig. 5. Noise figure measured using the simplified RCN, compared with a reference measurement and original RCN result from [9]

depend on a chamber-loss measurement, so it has one less uncertainty contribution. This is a significant improvement, since the chamber-loss measurement uncertainty can be in the order of 0.5 dB [10], but this is heavily dependent on the setup. We estimate the uncertainty of the final result with a Monte-Carlo simulation, considering the uncertainty of each separate measurement and using a 2.45 coverage factor, comparable to [9].

The results of the measured noise figure and gain are shown in Fig. 5 and 6, respectively, including error bars. It can be seen that the uncertainty of the simplified RCN noise-figure estimate overlaps with the reference and the original RCN results, showing that there is no significant difference between them. However, the simplified RCN gain result does not overlap in two narrow parts of the band with the reference, and the original RCN gain result is, overall, closer to the reference. We expect that this is because a different horn antenna and waveguide-to-coaxial adapter were used, as compared to the reference and original RCN measurements in [9], as mentioned in Section III. The expanded uncertainty in the original RCN was 0.67 dB for NF an 1.00 dB for gain. For the simplified RCN this is approximately 0.37 dB for NF and 0.75 dB for gain, showing the reduction in uncertainty due to the need for one less calibration step.

IV. Conclusion

We introduced a simplified version of the RCN method for over-the-air noise-figure and gain measurements of integrated devices. The simplification uses two instead of three calibrations steps, which is achieved by having both the calibration antenna and DUT inside the chamber. This omits the need for a vector network analyzer in this method, and all measurements can be performed using a spectrum analyzer.

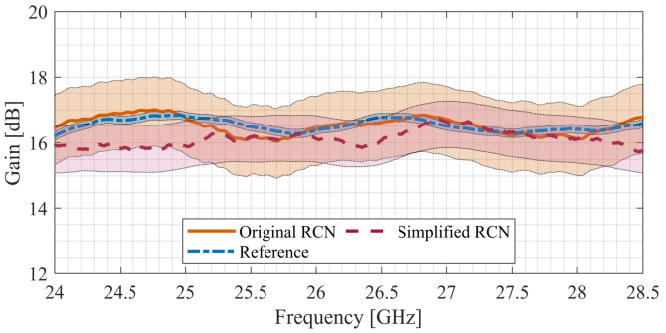

Fig. 6. Gain measured using the simplified RCN, compared with a reference measurement and original RCN result from [9]

This reduced the expanded uncertainty in the noise-figure and gain estimates by 0.3 dB and 0.25 dB, respectively, to 0.37 dB and 0.75 dB. The measured results of the DUT are within the uncertainty bounds of the reference value, and of the original RCN result. The method is user-friendly, and can also be applied in lower-frequency chambers, and for DUTs with a lower noise figure. Additionally, since the (simplified) RC estimates the NF and gain of the complete device, effects such as noise matching are taken into account in the measurement.

ACKNOWLEDGMENT

The authors would like to acknowledge David Prinsloo, Ulf Johanssen, Ad Reniers, Simon Rommel, Roel Budé, Niels Vertegaal, and Gabriele Federico for their technical assistance.

REFERENCES

[1] M. E. Tiuri, "Radio Astronomy Receivers," pp. 930–938, 1964.
[2] K. Kolb, J. Potschka, T. Maiwald, K. Aufinger, M. Dietz, and R. Weigel, "A 28 GHz Broadband Low Noise Amplifier in a 130 nm BiCMOS Technology for 5G Applications," in *2020 23rd International Microwave and Radar Conference, MIKON 2020*. Institute of Electrical and Electronics Engineers Inc., 10 2020, pp. 192–195.
[3] D. M. Pozar and B. Kaufman, "Comparison of Three Methods for the Measurement of Printed Antenna Efficiency," *IEEE Transactions on Antennas and Propagation*, vol. 36, no. 1, pp. 136–139, 1988.
[4] J. Ashkenazy, E. Levine, and D. Treves, "Radiometric measurement of antenna efficiency," *Electronics Letters*, vol. 21, no. 3, p. 111, 1985.
[5] Joel P. Dunsmore and Keysight Technologies, "OTA G/T Measurements of Active Phased Array Antenna Noise using a Vector Network Analyzer," Tech. Rep., 2020.
[6] Institute of Electrical and Electronics Engineers and Antenna Standards Committee, *IEEE standard test procedures for antennas*. Institute of Electrical and Electronics Engineers, 1979.
[7] E. Franke, "Effects of solar, galactic and man-made noise on UHF SATCOM operation," in *Proceedings - IEEE Military Communications Conference MILCOM*, vol. 1. IEEE, 1996, pp. 29–36.
[8] D. C. Hogg and R. A. Semplak, "The Effect of Rain and Water Vapor on Sky Noise at Centimeter Wavelengths," Tech. Rep., 1961.
[9] T. Stek, A. Hubrechsen, D. S. Prinsloo, and U. Johannsen, "Over-the-air noise figure characterization of mm-wave active integrated antennas using a reverberation chamber," *IEEE Transactions on Microwave Theory and Techniques*, pp. 1–9, 2022.
[10] A. Hubrechsen, K. A. Remley, and S. Catteau, "Reverberation chamber metrology for wireless internet of things devices: Flexibility in form factor, rigor in test," *IEEE Microwave Magazine*, vol. 23, no. 2, pp. 75–85, 2022.
[11] CTIA Certification, "Test plan for wireless large-form-factor device over-the-air performance, version 1.2.1," November 2020.
[12] C. L. Holloway, H. A. Shah, R. J. Pirkl, W. F. Young, D. A. Hill, and J. Ladbury, "Reverberation chamber techniques for determining the radiation and total efficiency of antennas," *IEEE Transactions on Antennas and Propagation*, vol. 60, no. 4, pp. 1758–1770, Apr 2012.
[13] A. Hubrechsen, S. J. Verwer, R. Ad C. F., L. A. Bronckers, and A. B. Smolders, "Pushing the boundaries of antenna-efficiency measurements towards 6g in a mm-wave reverberation chamber," in *2021 IEEE Conference on Antenna Measurements Applications (CAMA)*, 2021, pp. 263–265.